Electron-electron scattering in far-infrared quantum cascade lasers

Per Hyldgaard* and John W. Wilkins
Department of Physics, 174 West 18th Avenue, Ohio State University, Columbus, Ohio 43210-1106
(Received 20 November 1995)

A large depolarization shift indicates a strong *nonequilibrium* intersubband electron-electron scattering (Γ) in tunneling structure. For a far-infrared subband separation $\Delta\sim 10$ meV, the rate Γ scales with the upper-subband occupation and is never significantly reduced by screening. Despite this nonradiative decay a finite population inversion can be maintained. Finally, the applied bias changes the wave-function symmetry so as to cause a dramatic variation of the electron-electron scattering rate.

In the quantum cascade laser[1] a nonequilibrium current injection exclusively into the upper subband of a multiple-level tunneling structure provides a finite *intersubband* population inversion and actual lasing (at midinfrared frequency $\omega\sim 300$ meV). This seminal achievement culminates a search begun in 1971 with the proposal by Kazarinov and Suris[2] soon after the groundbreaking work by Esaki and Tsu.[3] There is also a considerable interest in the far-infrared (or Terahertz) regime and we mention in particular the observation[4] of spontaneous intersubband emission in superlattices excited by a current flow. Adapting the quantum-cascade-laser design[1] we presently investigate the population inversion in a tunneling structure with far-infrared subband separation, $\Delta\approx 11$ meV.

The prospect of such far-infrared stimulated emission is raised by the small intersubband decay, $1/\tau\lesssim 0.03$ meV, observed[5] at temperatures $T\lesssim 50$ K and at weak optical pumping.[6] This small decay is possible because the optical-phonon frequency ($\Omega_{\rm LO}\approx 36$ meV in GaAs) exceeds the subband separation, $\Delta\approx 11$ meV, and optical-phonon emission processes are inhibited[5] at temperatures below the activation energy $\Omega_{\rm LO}-\Delta\approx 25$ meV.

We find, however, that the current injection results in a strong *nonequilibrium* electron-electron intersubband scattering (Γ) which we evaluate for a complete upper-subband occupation below the emitter chemical potential. This scattering Γ is never significantly reduced by screening and, unlike the near-equilibrium electron-electron scattering,[7] is *not* inhibited by the Pauli exclusion (as we can assume population inversion.) In this letter we (1) identify a simple scaling of the nonequilibrium electron-electron scattering rate (Γ) with the upper-subband occupation, (2) predict a very strong intersubband decay $\sim 2\Gamma\approx 1.0$ meV for an upper-subband sheet density $N_L\approx 10^{11}$ cm^{-2} comparable to that in the mid-infrared quantum cascade laser,[1] (3) demonstrate that a smaller population inversion density ($\sim 0.17\times 10^{11}$ cm^{-2}) *can* be maintained at a moderate tunneling current density, and finally (4) predict for the electron-electron scattering a dramatic bias dependence arising from the so-called quantum-confined Stark effect.[8]

A far-infrared quantum-cascade-laser design. The bottom panel of Fig. 1 shows the schematics of the far-infrared optically active tunneling structure presently investigated. We assume the tunneling is independent of the electron energy in the plane of the heterostructure layers $E_\parallel(k)=k^2/2m_e^*$. The top panel of Fig. 1 illustrates the intersubband scattering (Γ) between two upper-subband electrons $[E_2+E_\parallel(k)]$ to two lower-subband electrons $[E_1+E_\parallel(k)]$. For the current-injected upper-subband occupation density n_2 the lower-subband occupation n_1 results from the net nonradiative decay $n_2\Gamma_{\rm nr}$.

The subband occupation densities are determined from the two-level rate equation involving additional tunneling rates[9]—Γ_e, Γ_{c1}, and Γ_{c2}—illustrated in Fig. 1:

$$\frac{dn_2}{dt}=(N_L-n_2)\Gamma_e-n_2\Gamma_{c2}-n_2\Gamma_{\rm nr},$$
$$\frac{dn_1}{dt}=n_2\Gamma_{\rm nr}-n_1\Gamma_{c1}. \tag{1}$$

There is no current injection into the lower subband because the lower band edge ϕ_L of the emitter is raised above E_1. The steady-state solution of Eq. (1) thus yields $n_2-n_1\propto N_L(1-\Gamma_{\rm nr}/\Gamma_{c1})$, and population inversion requires $\Gamma_{c1}>\Gamma_{\rm nr}$. The lower-level escape rate $\Gamma_{c1}\sim 0.5$ meV is significantly larger than the decay rate $1/\tau\approx 0.03$ meV measured under a weak optical pumping.[6] Here we investigate the nonequilibrium electron-electron scattering to test if population inversion can be maintained.[10]

Effective Coulomb interaction. The characteristic in-plane momentum transfer $q_\Delta=\sqrt{2m_e^*\Delta}$ together with the zero-frequency background dielectric constant ϵ_0 provides a natural scaling of the effective Coulomb interaction $(e^2/\epsilon_0 q_\Delta^2)U(q)$, where $U(q)$ is a dimensionless matrix element introduced below. For the screened $U(q)$ and unscreened $U^0(q)$ matrix element we find (a) a moderate q variation, (b) a correspondingly moderate dependence on an effective Thomas-Fermi screening[11] wave vector $q_{\rm TF}$, and (c) a numerical value of $U^0(q=0)$ that can be estimated from experiments.[5]

The screened effective dimensionless matrix element is defined

$$\begin{aligned}U(q)\equiv U_{21,21}(q)=2\pi\int dx_2\int dx_1\Psi_2(x_2)\Psi_1(x_2)q_\Delta\\ \times\exp(-\sqrt{q^2+q_{\rm TF}^2}|x_2-x_1|)/\sqrt{q^2+q_{\rm TF}^2}\\ \times\Psi_2(x_1)\Psi_1(x_1),\end{aligned} \tag{2}$$

in terms of the resonant-level wave functions[12] and Thomas-Fermi wave vector q_{TF}. The unscreened interaction matrix element $U^0(q)$, the $q_{\mathrm{TF}}\to 0$ limit of (2), is finite at $q=0$. The moderate variation of $U^0(q)$, namely $U^0(q_\Delta)\approx U^0(0)/4$, can be deduced analytically for a square quantum well with infinite barriers. That the screening is ineffective in modulating the nonequilibrium electron-electron scattering follows directly from the observation $U(q)=U^0(\sqrt{q^2+q_{\mathrm{TF}}^2})$ because the estimated Thomas-Fermi screening wave vector remains smaller than the characteristic momentum transfer,[11] $q_{\mathrm{TF}}<q_\Delta$.

Finally, the *strength* of the effective nonequilibrium electron-electron interaction is evident from the observed[5] large equilibrium depolarization shift[13,14] $\Delta^*-\Delta\approx 2$ meV of the absorption peak, Δ^*, from the far-infrared subband separation $\Delta\approx 11$ meV at sheet density $N_s\approx 10^{11}$ cm^{-2}. In particular, neglecting the coupling to other quantum levels, we have[11,14]

$$(\Delta^*)^2-\Delta^2=2\Delta N_s(e^2/\epsilon_0 q_\Delta)U^0(q=0). \tag{3}$$

For a finite occupation density $n_2\lesssim N_L\sim N_s\approx 10^{11}$ cm^{-2} we thus expect the strong interaction $N_L(e^2/\epsilon_0 q_\Delta)U^0(0)\lesssim 2$ meV.

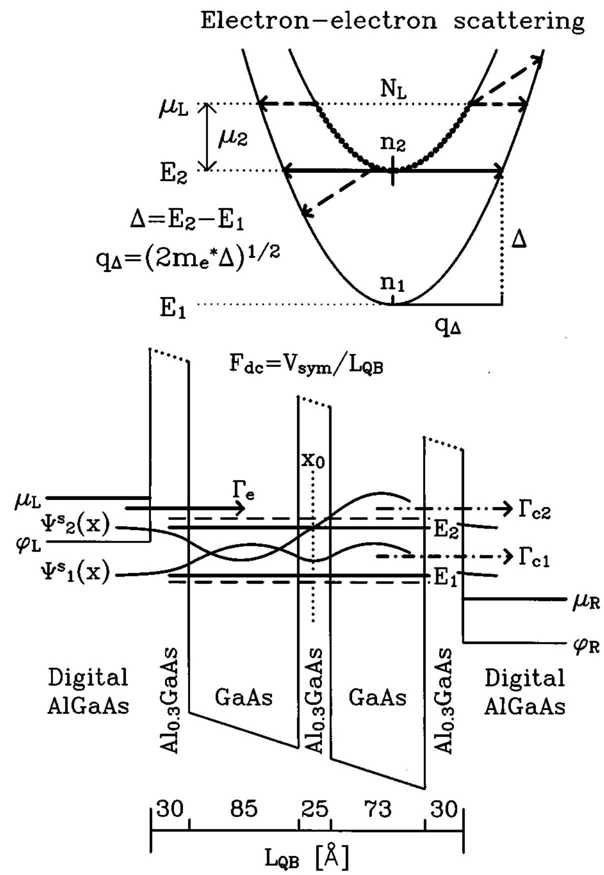

FIG. 1. Schematic (bottom panel) of far-infrared quantum-cascade-laser design *and* (top panel) of nonequilibrium electron-electron scattering Γ. The hypothetical tunneling structure comprises an asymmetric double-quantum-well region[5] surrounded by the n-doped (left/right) emitter/collector leads. A moderate voltage drop $V\equiv(\mu_L-\mu_R)/e\sim 20$ mV ensures a current injection Γ_e exclusively into upper resonant level E_2 and fast tunneling escape rates[9] Γ_{c1} and Γ_{c2} out of levels E_1 and E_2, respectively. Bottom panel shows tunneling potential and resonant levels at voltage drop V_{sym} with (a) minimal subband separation ($\Delta\equiv E_2-E_1$) and (b) near-exact inversion symmetry of corresponding wave functions, $\Psi_1^s(x)$ and $\Psi_2^s(x)$. The three pairs of opposite transition arrows in the top panel illustrate the nonequilibrium scattering Γ between two upper-subband electrons which both decay to subband E_1. As indicated by the pair of solid arrows, the scattering Γ occurs with the characteristic momentum transfer $q_\Delta=\sqrt{2m_e^*\Delta}$ and on average with no energy transfer.

Scaling of electron-electron scattering. We use the Fermi golden rule[15] to evaluate the total rate Γ for two (opposite-spin[16]) upper-subband electrons to decay to subband E_1. For complete upper-subband occupation (i.e., $n_2=N_L$) at zero temperature we obtain Γ as a sum over the in-plane momentum transfer q of the squared matrix element $[|U(q)|^2]$ weighted by the phase-space contribution $[P(q)]$ introduced below. Because, however, $|U(q)|^2$ exhibits only a moderate q variation and because the scattering phase space is dominated by the contribution at q_Δ, we can approximate[17]

$$\Gamma\approx\frac{\mathrm{Ry}^*}{\pi^2}\left(\frac{\mu_2}{\Delta}\right)|U(q_\Delta)|^2 I_P(\mu_2/\Delta), \tag{4}$$

where

$$I_P(\mu_2/\Delta)\equiv\int\frac{dq}{k_{\mu_2}}\frac{q}{k_{\mu_2}}P(q)\approx I_P(0)=0.785 \tag{5}$$

represent a dimensionless integrated phase-space measure essentially independent of μ_2/Δ.

The top panel of Fig. 2 verifies linear-in-μ_2 scaling of Γ, as expressed in Eqs. (4) and (5). For the unscreened interaction the linear scaling is nearly exact and closely approximated by $\mathrm{Ry}^*/\pi^2(\mu_2/\Delta)|U^0(q_\Delta)|^2 I_P(0)$. For the screened rate ($q_{\mathrm{TF}}>0$), there is some deviation arising from the increasing screening of squared matrix element $|U(q)|^2$. At most, that screening causes a factor of 2 reduction even at $\mu_2=\Delta$.

To explain the central result Eq. (4) we consider the phase-space contribution at momentum transfer q (see also Ref. 15),

$$N_L^2\mu_2^{-1}P(q)=\frac{1}{2}\sum_{\vec{k},\vec{k}'}\Theta(\mu_2-E_\parallel(k))\times\Theta(\mu_2-E_\parallel(k'))2\pi\delta(E_f-E_i). \tag{6}$$

The displayed one-half factor arises because we only consider direct scattering between opposite-spin electrons.[16] The energy difference, E_f-E_i, between the final and initial state depends on q and on the initial in-plane momenta, $\vec{k}$ and $\vec{k}'$. In Ref. 11 we show that the *weighted* dimensionless phase-space contribution, $(q/k_{\mu 2})P(q)$, (a) has the domain $-1\leqslant q/k_{\mu_2}-\sqrt{1+(q_\Delta/k_{\mu_2})^2}\leqslant 1$, (b) is always strongly peaked at the characteristic momentum transfer q_Δ with constant maximum value $(q_\Delta/k_{\mu_2})P(q_\Delta)=8/(3\pi)$, and consequently, (c) results in an almost μ_2/Δ-independent integrated phase-space measure, $I_P(\mu_2/\Delta)\approx I_P(0)$.

The key observation is (b), which follows from the assumed quadratic subband dispersion, $E_\parallel(k)$. Specifically, at

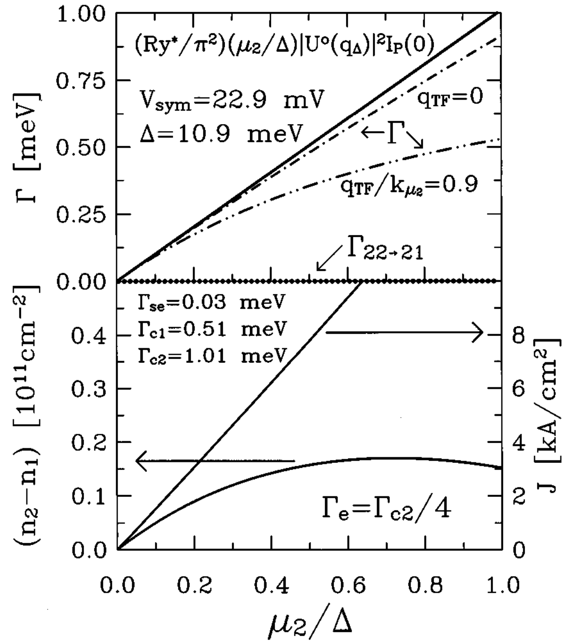

FIG. 2. Top panel shows the approximate scaling, solid curve, with electron occupation μ_2/Δ of unscreened (screened) nonequilibrium scattering rate Γ, dashed–single-(double-) dotted curve. Screening causes at most a factor of 2 reduction of Γ even at $\mu_2=\Delta$. The interaction matrix elements are evaluated at $V_{\rm sym}$ where the rate[17] $\Gamma_{22\to21}$, dotted curve, essentially vanishes. Bottom panel demonstrates[19] that a finite population inversion (left axis) $n_2-n_1 \gtrsim 0.17\times10^{11}$ cm^{-2} can be maintained at a moderate current density (right axis) $J=e\Gamma_e(N_L-n_2)$ despite the strong intersubband scattering. Note, however, that the population inversion quickly saturates and eventually decreases, whereas the current density $J=eN_L(1-n_2/N_L)$ shows a faster-than-linear increase with μ_2/Δ.

the characteristic momentum transfer, $q=q_\Delta$, the δ-function argument, (E_f-E_i), in Eq. (6) reduces to $(q_\Delta(k_y-k_y')/m_e^*)$, where we have chosen the y direction to be parallel to the in-plane momentum transfer. The phase-space contribution, Eq. (6), then scales as $m_e^* k_{\mu_2}^3/q_\Delta$ and (upon extracting $N_L^2\mu_2^{-1}\propto m_e^* k_{\mu_2}^2$) we arrive at the constant value $(q_\Delta/k_{\mu_2})P(q_\Delta)=8/(3\pi)$.

A finite population inversion. The bottom panel of Fig. 2 estimates the population inversion n_2-n_1 (left axis) and the current density $J=e\Gamma_e(N_L-n_2)$ (right axis). These estimates are based on the steady-state solution of Eq. (1) using the simple assumption,

$$\Gamma_{\rm nr}(n_2)=\Gamma_{\rm se}+2\left(\frac{n_2}{N_L}\right)\frac{\mathrm{Ry}^*}{\pi^2}\left(\frac{\mu_2}{\Delta}\right)|U^0(q_\Delta)|^2 I_P(0), \quad (7)$$

for the total intersubband decay rate at voltage drop $V_{\rm sym}$. We assume[18] in Eq. (7) the total single-electron decay rate $\Gamma_{\rm se}$ bounded by the value, $1/\tau\approx0.03$ meV, measured[5] at weak optical pumping and $T=50$ K. The estimate, $\Gamma_{\rm nr}(n_2)-\Gamma_{\rm se}$ for the electron-electron decay results as follows. The scattering[17] $\Gamma_{22\to21}$ can be neglected at $V_{\rm sym}$. The scattering Γ removes two electrons at a time but is reduced by the partial upper-subband distribution $f_2(k)\equiv(n_2/N_L)\times\Theta(\mu_2-E_\parallel(k))$. Finally, we approximate the resulting electron-electron decay $2(n_2/N_L)\Gamma$ by the scaling result (solid curve in top panel) for Γ.

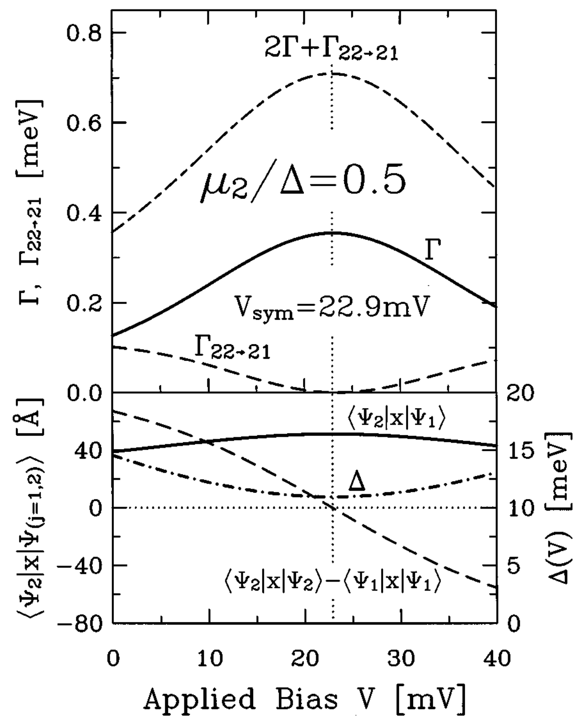

FIG. 3. Dramatic voltage-drop variation (top panel) of electron-electron scattering rates, Γ and[17] $\Gamma_{22,21}$, explained (bottom panel) by the quantum-confined Stark effect[8] on the wave-function overlap and symmetry. Bottom panel identifies $V_{\rm sym}$ (vertical dotted line) as the voltage drop with minimal subband separation (dash-dotted curve). Observe that the dipole matrix element (solid curve) is nearly constant, whereas the center-of-charge separation (dashed curve) vanishes[20] at $V_{\rm sym}$. The bias dependence of Γ and $\Gamma_{22\to21}$ reflects the wave-function-symmetry dependence of the characteristic matrix element $|U^2(q_\Delta)|^2$ and $|U^2_{22,21}(q_\Delta/\sqrt{2})|^2$, respectively. In particular, the matrix element $U(q_\Delta)$ and thus Γ enhance at $V_{\rm sym}$ because of the increased wave-function overlap. In contrast, the matrix element $U_{22,21}(q_\Delta/\sqrt{2})$ and thus $\Gamma_{22\to21}$ are strongly reduced close to $V_{\rm sym}$ but increase dramatically when, for $V\neq V_{\rm sym}$, the wave-function symmetry is lost. Finally, the upper panel shows the combined electron-electron scattering rate, $2\Gamma+\Gamma_{22\to21}$, which also exhibits a significant wave-function-symmetry variation.

The current injection in the midinfrared quantum cascade laser[1] maintains a population inversion $n_2\approx N_L\sim10^{11}$ cm^{-2} which requires $\mu_2\approx5$ meV and $\Gamma_e\gg\Gamma_{c2}$. In the present far-infrared structure the resulting strong decay $2\Gamma\approx1.0$ meV would eliminate such a population inversion. Nevertheless, Fig. 2 demonstrates[19] that a smaller population inversion, $n_2-n_1\gtrsim0.17\times10^{11}$ cm^{-2} can be maintained at current densities comparable to the midinfrared quantum cascade laser.[1]

However, also note the population inversion, n_2-n_1, quickly saturates and eventually decreases whereas the current density, $J=e\Gamma_e N_L(1-n_2/N_L)$, shows a faster-than-linear increase with μ_2/Δ. A choice of $\Gamma_e\gg\Gamma_{c2}\approx1.0$ meV (not shown) does not increase the maximum population inversion and causes a strongly nonlinear rise of the current with μ_2/Δ. The electron-electron scattering thus forces a nontrivial optimization of Γ_e/Γ_{c2} and μ_2/Δ.

Wave-function-symmetry dependence. The bottom panel of Fig. 3 shows the so-called quantum-confined Stark effect[8] of the bias voltage on the subband separation and on the wave-function overlap and symmetry.[20] The minimal subband separation occurs at voltage drop V_{sym} (vertical dotted line). The dipole matrix element, $|\langle\Psi_2|x|\Psi_1\rangle|$ (solid curve), enhances at V_{sym} with the increased wave-function overlap. In contrast, the center-of-charge separation, $\langle\Psi_2|x|\Psi_2\rangle - \langle\Psi_1|x|\Psi_1\rangle$ (dashed curve) vanishes at V_{sym} but rapidly changes with $V-V_{\mathrm{sym}}$, a variation reflecting the loss of wave-function inversion symmetry.

The top panel of Fig. 3 shows the dramatic voltage-drop dependence of both scattering rate Γ (solid curve) and of $\Gamma_{22\to21}$ (dashed curve).[17] This variation reflects the wave-function-symmetry dependence of the characteristic matrix elements for a constant ratio $\mu_2/\Delta=\frac{1}{2}$; see Eq. (4) (cf. Ref. 17). In particular, the matrix element $U(q_\Delta)$, containing an even number of upper-level wave functions, can never be zero, and in fact enhances at $V=V_{\mathrm{sym}}$. In contrast, the characteristic matrix element $U_{22,21}(q_\Delta/\sqrt{2})$, containing three upper-level wave functions, must vanish close to V_{sym} (due to the near-exact wave-function inversion symmetry), but increases rapidly with the finite charge separation at $V\neq V_{\mathrm{sym}}$.

Finally, the top panel of Fig. 3 shows the *total* electron-electron decay, $2\Gamma+\Gamma_{22\to21}$, which also depends significantly on the wave-function-inversion symmetry. Ensuring an upper-subband current injection at $V\neq V_{\mathrm{sym}}$, may thus enhance the population inversion beyond the value, $n_2-n_1\approx 0.17\times 10^{11}$ cm^{-2}, estimated in Fig. 2.

The authors appreciate useful discussions with F. Capasso, S. P. Hershfield, G. D. Mahan, R. A. Smith, C. J. Stanton, and at UCSB with J. R. Allen, Jr., K. Craig, J. Heyman, M. Sherwin, and K. Unterrainer. We thank ITP, QUEST, and Material Research Laboratory at UCSB for their kind hospitality and the use of computer facilities during our visit. This work was supported by the Danish Natural Science Research Foundation and by the Office of Naval Research.

---

*Present address: Solid State Division, Oak Ridge National Lab, P.O. Box 2008, Oak Ridge, TN 37831.

[1] J. Faist, F. Capasso, D. L. Sivco, C. Sirtori, A. L. Hutchinson, and A. Y. Cho, Science **264**, 553 (1994); J. Faist, F. Capasso, D. L. Sivco, A. L. Hutchinson, C. Sirtori, S. N. G. Chu, and A. Cho, Appl. Phys. Lett. **65**, 2901 (1994).

[2] R. F. Kazarinov and R. A. Suris, Fiz. Tekh. Poluprovodn. **5**, 797 (1971) [Sov. Phys. Semicond. **5**, 707 (1971).]

[3] L. Esaki and R. Tsu, IBM J. Res. Dev. **14**, 61 (1970).

[4] M. Helm, P. England, E. Colas, F. DeRosa, and S. J. Allen, Jr., Phys. Rev. Lett. **63**, 74 (1989).

[5] J. N. Heyman, K. Unterrainer, K. Craig, B. Galdrikian, M. S. Sherwin, K. Campman, P. F. Hopkins, and A. C. Gossard, Phys. Rev. Lett. **74**, 2682 (1995). The experimentally investigated isolated quantum-well sample constitutes the central region of our hypothetical far-infrared tunneling structure; see Fig. 1.

[6] Reference 5 also reports a moderate decay rate ($1/\tau\approx 0.05$ meV at $T=10$ K) under a strong optical pumping. A comparison requires, however, a detailed modeling of the optically excited electron gas and is not presently undertaken.

[7] V. I. Fal'ko, Phys. Rev. B **47**, 13 585 (1993); P. Sotirelis, *ibid*. **47**, 12 744 (1993).

[8] D. A. B. Miller, D. S. Chelma, T. C. Damen, A. C. Gossard, W. Wiegmann, T. H. Wood, and C. A. Burrus, Phys. Rev. Lett. **53**, 2173 (1984).

[9] We estimate [see J. Bardeen, Phys. Rev. Lett. **6**, 57 (1961) and N. S. Wingreen, Ph.D. dissertation, Cornell University, 1989] $\Gamma_{c1(c2)}\approx(v_{1(2)}/2L_{\mathrm{QB}})T_R(E_{1(2)})$ with velocity $v_{1(2)}=\sqrt{2E_{1(2)}/m_e^*}$, transmission probability $T_R(E)=\sqrt{E(E-\phi_R)}\exp[-2L_B\sqrt{2m_e^*(\phi_B-E)}]/(\phi_B-E)$, lower collector band edge ϕ_R, and assuming a $L_B=30$ Å ($\phi_B=214$ meV) barrier thickness (height.) For the structure shown in Fig. 1 we predict only a $\Gamma_{c1(c2)}=0.40(0.93)$ meV to $\Gamma_{c1(c2)}=0.56(1.09)$ meV variation within the range $12\lesssim V\lesssim 30$ mV of voltage drops ensuring the upper-subband current injection. We neglect electron charging effects in these estimates of $\Gamma_{c1,c2}$, noting that a 10^{11} cm^{-2} electron sheet density causes just a 10% change in the internal field $\approx V/L_{\mathrm{QB}}$ at $V\sim 20$ mV. The moderate variation in $\Gamma_{c1,c2}$ can be negated by a small change in the barrier thickness.

[10] The strong nonequilibrium electron-electron scattering may also affect the study [see, for example, A. N. Korotkov, D. V. Averin, and K. K. Likharev, Phys. Rev. B **49**, 7548 (1994)] of possible continuous Bloch oscillations in a two-level tunneling structure.

[11] P. Hyldgaard, Ph.D. dissertation, Ohio State University, 1995.

[12] We thank Dr. B. Galdrikian for kind permission to use his Schrödinger-solver code.

[13] S. J. Allen, Jr., D. C. Tsui, and B. Vinter, Solid State Commun. **20**, 425 (1976).

[14] Q. P. Li and S. Das Sarma, Phys. Rev. B **43**, 11 768 (1991); Ben Yu-Kuang Hu and S. Das Sarma, *ibid*. **48**, 5469 (1993).

[15] The rate Γ is defined by $\{AN_L\}\Gamma\equiv\Sigma_{\vec{q}}(e^2/\epsilon_0 q_\Delta)^2|U(q)|^2N_L^2\mu_2^{-1}P(q)$ with phase-space contribution $N_L^2\mu_2^{-1}P(q)$ listed in Eq. (6).

[16] We assume for the same-spin scattering that the moderate variation of $U(q)$ causes the direct and exchange contribution to approximately cancel.

[17] We also evaluate (for $n_2=N_L$) the scattering $\Gamma_{22\to21}$ between two-subband E_2 electrons of which only one decays to subband E_1. This rate can be approximated as Eq. (4) but with a different characteristic matrix element $U_{22,21}(q_\Delta/\sqrt{2})$ (defined by three upper-level wave functions) and phase-space measure (Ref. 11) $I_{22\to21}(\mu_2/\Delta)$. There is no scaling of $\Gamma_{22\to21}$ because the Pauli exclusion (within subband E_2) restricts the phase space ($I_{22\to21}$) for $\mu_2/\Delta>\frac{1}{8}$; see Ref. 11.

[18] The intersubband decay due to impurity, interface defect, and acoustic-phonon scattering remains at temperature $T\leqslant 50$ K strictly bounded by the experimental value $1/\tau=0.03$ meV. We estimate the decay due to thermally activated optical-phonon emission bounded at 10^{-3} meV for $T\leqslant 25$ K.

[19] We take $\Gamma_{c1(c2)}=0.51(1.01)$ meV (estimated at V_{sym}) and use $\Gamma_e=\Gamma_{c2}/4$.

[20] J. Faist, F. Capasso, A. L. Hutchinson, L. Pfeiffer, and K. W. West, Phys. Rev. Lett. **71**, 3573 (1993); this paper reports and explains the corresponding voltage-drop dependence of the optical selection rules.